Received: 7 October 2021 | Revised: 27 July 2022 | Accepted: 27 July 2022 | Published on: 16 August 2022

DOI: 10.1002/joc.7820

RESEARCH ARTICLE

International Journal of Climatology RMetS

# Study on the classification and characteristics of cold surge in South Korea

**Eung-Sup Kim**[1] | **Joong-Bae Ahn**[2]

[1]Department of Atmospheric Sciences, BK21 School of Earth and Environmental Systems, Pusan National University, Busan, South Korea

[2]Department of Atmospheric Sciences, Pusan National University, Busan, South Korea

**Correspondence**
Joong-Bae Ahn, Division of Earth Environmental System, Pusan National University, 2, Busandaehak-ro 63beon-gil, Geumjeong-gu, Busan 46241, South Korea.
Email: jbahn@pusan.ac.kr

**Funding information**
Korea Meteorological Administration, Grant/Award Number: KMI2020-01411

**Abstract**

This study examined the characteristics of cold surges in the Korean Peninsula over the last 45 years (1975–2019). During the period, there were 37 cases of cold surges affected by blocking (B_CS) and 129 cases of cold surges not influenced by blocking (nB_CS), indicating that most of the cold surges were nB_CS. The blocking that caused a cold surge over the Korean peninsula occurred mostly in the Okhotsk region and Ural region (OK_B and UR_B, respectively). In rare cases, blocking occurred simultaneously in the two regions called double blocking (DO_B), causing strong and long-lasting cold surges. The nB_CS was related closely to the propagating wave-train, hence the mean duration of nB_CS was shorter than the B_CS because the wave-train propagated fast from the northwest to the southeast. Although the number of occurrences of B_CS was low, B_CS was stronger and lasted longer than nB_CS. In the case of cold surges affected by UR_B, referred to as UR_CS, their progression was slower compared to the cold surges affected by nB_CS because UR_B is slowing the atmospheric flow in the west. For cold surges affected by OK_B (OK_CS), the progression was slower than nB_CS and UR_CS because blocking was located downstream, slowing the propagating trough. Accordingly, the mean durations of nB_CS, UR_CS, and OK_CS were 2.7, 3.6, and 5.1 days, respectively, the mean of the temperature anomaly throughout the cold surge, was −3.8, −5.4, and −5.1°C, respectively. Overall, both the intensity and the progression speed of the cold surges differed according to the presence and location of blocking. A common characteristic of all types of cold surges was that they occur after the passage of the trough having a baroclinic structure. In addition, all types of cold surges were linked to an expansion of the Siberian high.

**KEYWORDS**

cold surge, Okhotsk blocking, the Korea peninsula, Ural blocking, wave-train

# 1 | INTRODUCTION

A cold surge is a phenomenon that occurs in winter in the mid- and high-latitudes, which damages crops and affects plant growth, reducing crop production. Cold surges can also cause human casualties, such as hypothermia, frostbite, and death by freezing. Some studies have reported that the mortality rate increases linearly with the duration of cold surges (Vavrus *et al.*, 2006; Barnett *et al.*, 2012). In addition, property damage can occur as a result of freezing or bursting caused by cold surges. Recently, climate change has been progressing rapidly, but the likelihood of sudden occurrences of cold surges is increasing. According to Ryoo *et al.* (2004), there have been no significant changes in the frequency of cold surges on the Korean Peninsula, even in a globally warming climate. Therefore, continuous research on winter cold surges is important, regardless of global warming.

In general, troughs can develop more deeply in East Asia and North America when the Arctic oscillation (AO) is in its negative phase. Moreover, cold surges occur frequently as the advection of cold air from the polar regions carries cold air southward along this trough (Hong *et al.*, 2008). Cold surges occurring in East Asia, including the Korean Peninsula, are strongly correlated with the variation of the East Asia Winter Monsoon (EAWM). They are also closely related to the variation of the Siberian high. Hence, when the Siberian high expands, the cold northerly wind flows along its edge into the Korean Peninsula and East Asian regions, causing rapid temperature drops (Chen *et al.*, 2002; Hong *et al.*, 2008; Park *et al.*, 2010a). Im and Ahn (2004) reported that in addition to the EAWM index and Siberian High Index (SHI), the AO index and Southern oscillation index strongly correlate with the variability of winter temperatures in the Korean Peninsula. Jeong and Ho (2005) reported that the AO in the negative phase strongly correlates with cold surges in East Asia. Kim and Ahn (2010) conducted an Empirical Orthogonal Function (EOF) analysis. They reported that the AO pattern is the most dominant mode in winter over the Korean Peninsula, together with the Western Pacific pattern and the Pacific-North American patterns in January and the Eurasian pattern in February. Woo *et al.* (2012) stated that the decadal variability in the East Asian winter temperature is also affected by AO. Park and Ahn (2016) reported that the AO and WP patterns affect the temperatures of the Korean Peninsula and East Asia significantly when they are in the same phase. In particular, the temperature decreases significantly when both patterns are in the negative phase. Several studies have shown that the weakening of the polar stratosphere circulation (Kim *et al.*, 2009) and the occurrence of the tropical Madden-Julian oscillation (Park *et al.*, 2010b) are linked to cold surges (Jeong *et al.*, 2016).

In recent years, several studies have examined the effect of Arctic sea ice in autumn on the decrease in temperature and the increase in the cold surge frequency in East Asia (Kim *et al.*, 2014; Yang *et al.*, 2020, 2021). Yang *et al.* (2020) showed that the cold surge in East Asia mainly originated from Europe before 1995, but from western Siberia after 1995. Pang *et al.* (2020) and (2022) investigated the influence of the Siberian blocking and negative phase of the Scandinavian pattern on the long-lived cold surges over the South China Sea, respectively. Several studies have made future projections for boreal winter cold temperatures and regional surges using the representative concentration pathway (RCP) and SSP scenarios through various model experimental projects, such as the Coupled Model Intercomparison Project (CMIP) and CORDEX projects. For example, Heo *et al.* (2018) showed future simulations, which the cold surge frequency decreased by 1.1 year$^{-1}$ by the late 21st century under the RCP 8.5 using CMIP Phase 5.

Studies on the association between blocking and cold surges have also been carried out. Wang *et al.* (2010) reported that Ural blocking has been closely associated with the Siberian high and the winter climate in East Asia since the 1970s. You and Ahn (2012) showed that the second EOF mode in the North Pacific in winter is related to North Pacific blocking and that the sea surface temperature (SST) around the Korean Peninsula is lower than their climatology during winter when the North Pacific blocking occurs frequently. Park *et al.* (2014) classified cold surges into wave-train and blocking types using the clustering method. They reported that the wave-train and blocking types have baroclinic and barotropic structures, respectively, with blocking type cold surges lasting longer than wave-train type cold surges. In addition, research has been conducted to develop an index to distinguish between these two types of cold surges using the potential vorticity and potential temperature (Park *et al.*, 2015). Cheung and Zhou (2016) reported a correlation between Ural blocking and the variability of the surface temperature in the EAWM region. They showed that the temperatures of East Asia are closely related to Ural blocking. Choi and Kim (2016) associated the blocking with the low temperatures that abnormally lasted for more than a month during the winters of 2010 and 2011.

Several studies have claimed that adiabatic heating due to an increase in the North Atlantic sea surface temperature (SST) forms a wave-train like pattern across North Atlantic and Europe to the Ural region, resulting in Ural blocking (Li, 2004; Sato *et al.*, 2014; Lim, 2015; Jin *et al.*, 2020). Luo *et al.* (2016) and Tyrlis *et al.* (2020) reported that the Warm-Arctic-Cold-Eurasia (WACE) pattern plays a significant role in the formation and development of Ural blocking. Hwang *et al.* (2020) suggested that the formation of blocking in the North Pacific region in winter is related to vorticity flux, which appears as a result of an interaction between high-and low-frequency eddies, which are background flows. In particular, they argued that the role of the jet is important because the peak of the high-frequency eddies is north of the jet stream exit. A wave train is formed in winter as the Rossby wave propagates on an Asian jet moving southward, and various factors, such as equatorial SST change and NAO, can affect the wave train. (Branstator, 2002; Hu *et al*., 2018). In particular, Hu *et al*. (2018) argued that fluctuations in the Eastern Pacific SST could help predict the formation of wave-train.

Blocking refers to a phenomenon in which the synoptic system becomes stagnant or has an anomalous path as airflow in the upper atmosphere is less zonal and has a large amplitude meandering in the north–south direction (Rex, 1950). Previous studies have shown that various factors, such as nonlinear effects of atmospheric motion, internal dynamics, and baroclinic transient eddies, are causes of the formation and maintenance of blocking, but the link is unclear (Shutts, 1983; Mullen, 1987; Nakamura and Wallace, 1993; Nakamura and Fukamachi, 2004). Blocking can cause long-lasting and abnormally low temperatures or snowfall over the blocked regions owing to such stagnant behaviours (Park *et al*., 2014, 2015; Bae and Min, 2016; Choi and Kim, 2016). Although the correlation between blocking and cold surges over the Korean Peninsula has been studied, most research was confined to case studies on the blocking related to the periods when cold surges occurred over the Korean Peninsula. In addition, blocking occurring in places, such as the Ural and Okhotsk regions, has a significant impact on the cold surge in the Korean Peninsula. On the other hand, few studies have classified cold surges in the Korean Peninsula according to the cause, and the location of blocking that causes the cold surges. Therefore, classifying cold surges affecting the Korean Peninsula according to the cause and location of blocking and identifying the characteristics for each classification can help predict cold surges. Therefore, this study examined the cold surges that occurred from 1975 to 2019 over the Korean peninsula, which were affected by blocking and the propagating wave-trains to determine the characteristics of each cold surge type. In addition, the characteristics of blocking-related cold surges were examined in terms of the location of the blocking.

# 2 | DATA AND METHODS

## 2.1 | Data

In this study, a cold surge is defined using the surface air temperature observed at the 56 in-situ Automated Surface Observing System (ASOS) stations of the Korean Meteorological Administration (KMA) in South Korea. Figure 1 presents the location of each weather station. In addition, the reanalysis daily mean data provided by the NCEP/NCAR (National Centers for Environmental Prediction/National Center for Atmospheric Research) are used to define blocking and perform synoptic analysis. The NCEP/NCAR reanalysis data have a grid interval of 2.5° in the horizontal direction and 17 isobaric levels in the vertical direction (Kalnay *et al*., 1996). The variables used in this study include the temperature at 2 m (T2m), temperature (T), geopotential height (Z), sea level pressure (SLP), and zonal wind data. The data periods for KMA ASOS and NCEP/NCAR reanalysis data are from 1975 to 2019.

## 2.2 | Definition of cold surge

Cold surges occur mainly when the Siberian high, which is dominantly located in the Eurasian continent in winter, expands, thereby introducing cold air towards the mid-latitude regions. For this reason, most studies have defined cold surges using the characteristics of a rapid fall in temperature along with the development of the Siberian high (Zhang *et al*., 1997; Chen *et al*., 2004; Jeong and Ho, 2005; Park *et al*., 2010a; 2014; 2015).

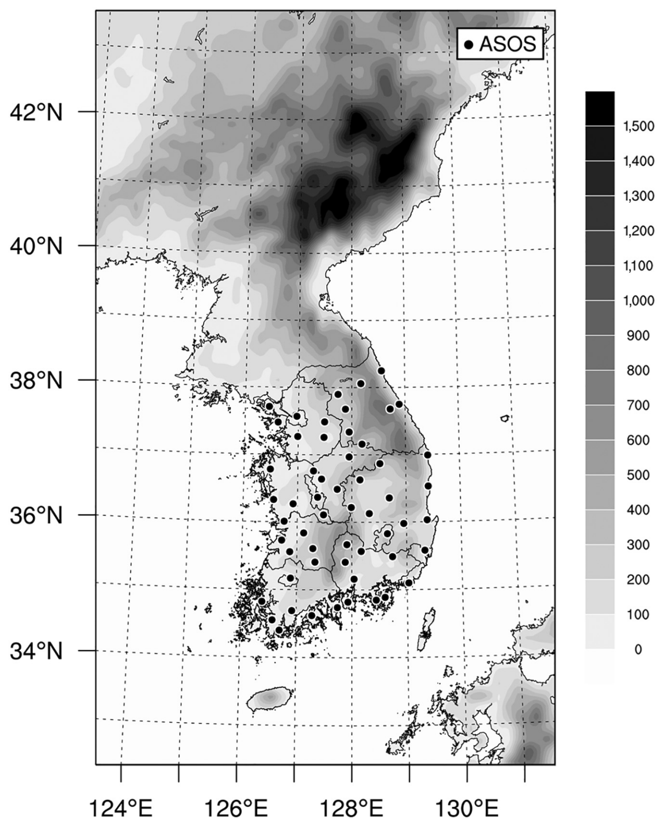


FIGURE 1 Locations of 56 ASOS in South Korea and topography (in metre)

In this study, the mean temperature in South Korea is calculated by averaging the surface air temperature of 56 in-situ ASOS observational stations. Based on previous studies, a cold surge is defined as a phenomenon in which the temperature of a day in boreal winter falls more than 1.5σ (standard deviation) within 2 days. Here, the standard deviation is obtained from daily variation in temperature during the boreal winter of 45 years. The termination day of the cold surge is defined as the day when the temperature increases again to higher than −0.5σ (Jeong and Ho, 2005; Park *et al.*, 2010a; 2014; 2015). 1.5σ and 0.5σ of the surface air temperature in South Korea in winter are approximately 5.7 and 1.9°C, respectively.

## 2.3 | Definition of blocking

Lejenäs and Økland (1983) proposed the blocking index, and Tibaldi and Molteni (1990) developed a new index called TM90 by supplementing it. The TM90 index is a method for analysing the presence of blocking for each longitude by calculating the difference between the 500 hPa geopotential height gradients (GHG) at north and south (GHGN and GHGS, respectively) based on 60°N in the latitudinal range from 40°N to 80°N. Barriopedro *et al.* (2006) proposed a modified blocking index by changing the latitude range of the TM90 index to 40°N–77.5°N. In this study, blocking is defined using the TM90 index proposed by Barriopedro *et al.* (2006) as follows:

$$\mathrm{GHGN}(\lambda)=\frac{Z(\lambda,\Phi_N)-Z(\lambda,\Phi_0)}{\Phi_N-\Phi_0}, \tag{1}$$

$$\mathrm{GHGS}(\lambda)=\frac{Z(\lambda,\Phi_0)-Z(\lambda,\Phi_S)}{\Phi_0-\Phi_S}, \tag{2}$$

where $\lambda$ and $\Phi$ are the longitude and latitude, respectively, and $Z(\lambda,\Phi)$ represents the 500 hPa geopotential height at $(\lambda,\Phi)$. $\mathrm{GHGN}(\lambda)$ and $\mathrm{GHGS}(\lambda)$ represent the 500 hPa geopotential height gradients at north and south at a given longitude, respectively. The equation for a given latitude can be expressed as follows:

$$\Phi_N=77.5^{\circ}\mathrm{N}+\Delta,$$

$$\Phi_0=60.0^{\circ}\mathrm{N}+\Delta,$$

$$\Phi_S=40.5^{\circ}\mathrm{N}+\Delta,$$

$$\Delta=-5.0^{\circ},-2.5^{\circ},0.0^{\circ},2.5^{\circ},\text{and } 5.0^{\circ}. \tag{3}$$

When the five values of $\Delta$ are applied, a given longitude is considered a longitude with blocking if both $\mathrm{GHGN}(\lambda)<-10\,\mathrm{gpm}\cdot\mathrm{lat}^{-1}$ and $\mathrm{GHGS}(\lambda)>0$ are satisfied at least once. When this condition is maintained for at least five consecutive days, it is finally considered to be blocking.

# 3 | RESULT AND DISCUSSION

## 3.1 | Classification of CS: Duration and intensity

The winter blocking frequency is relatively high over the North Atlantic, and North Pacific regions (dotted line in

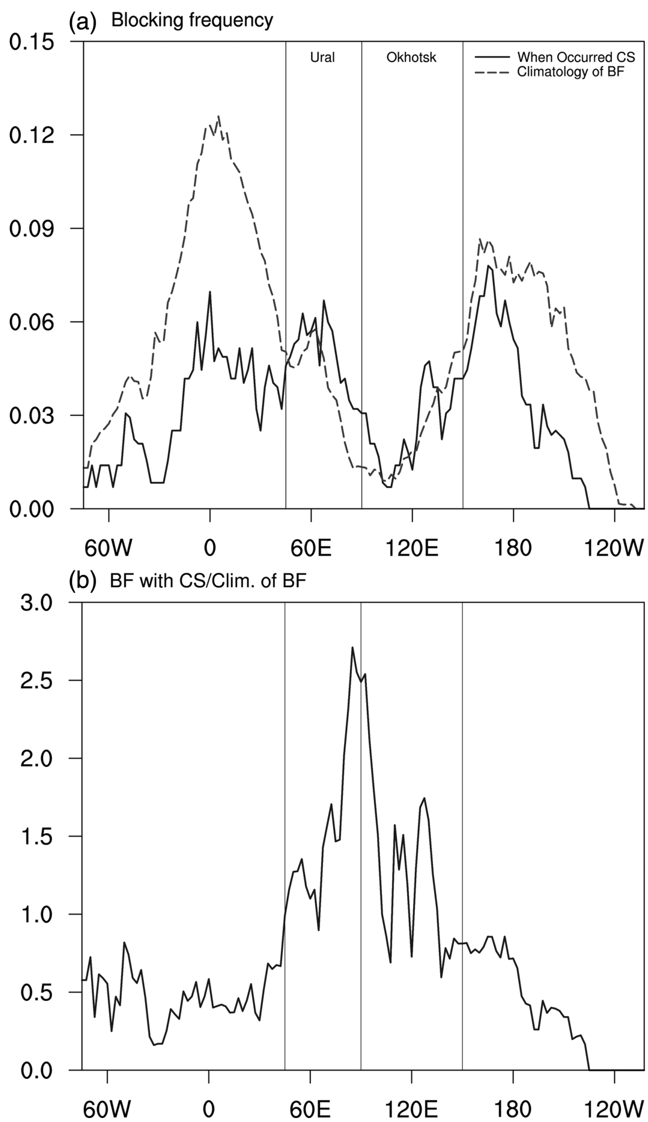


**FIGURE 2** (a) Climatology of the blocking frequency (dotted line) and blocking frequency when cold surge occurred in South Korea (solid line), and (b) ratio of blocking frequency when cold surge occurred in South Korea to the climatology of blocking frequency in the winters from 1975 to 2016 (41 years)

**TABLE 1** Summary of the cold surge in South Korea occurred over the last 45-years

| | | Blocking | | | |
|---|---|---|---|---|---|
| Type | Non-blocking (wave-train) | Ural | Okhotsk | Double | Total |
| Cases | 129 | 14 | 19 | 4 | 166 |
| Days | 352 | 51 | 97 | 47 | 547 |
| Duration | 2.7 | 3.6 | 5.1 | 11.8 | 3.3 |
| Ics[a] | −3.8 | −5.4 | −5.1 | −6.3 | −4.4 |

[a]Ics: Intensity of cold surge: temperature anomaly averaged during cold surge period (unit: °C).

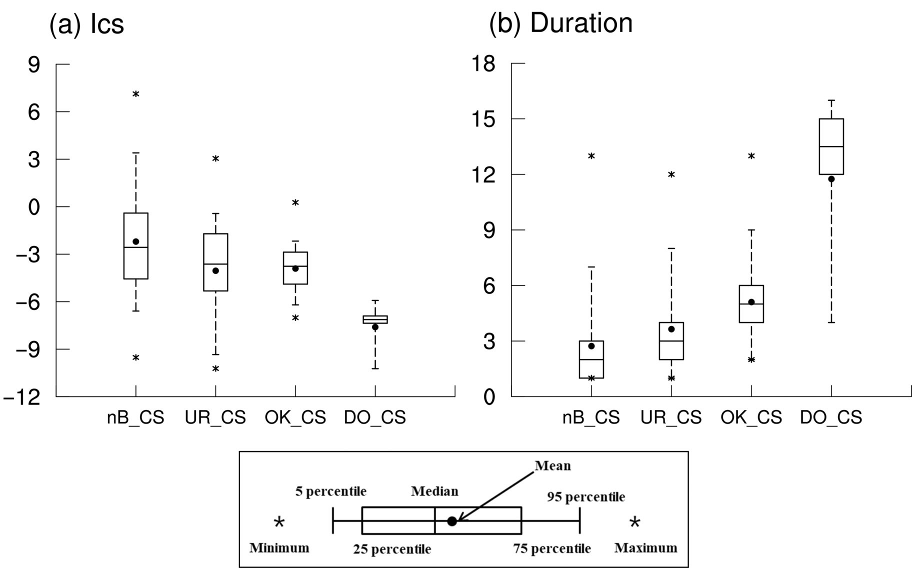


**FIGURE 3** Distribution of (a) intensity of cold surge, and (b) duration of the cold surge. The values are from 56 ASOS stations in South Korea

Figure 2a), which are similar to the distribution shown in previous studies (Tibaldi and Molteni, 1990; You and Ahn, 2012; Lee and Ahn, 2017). The blocking location and frequency are investigated when the cold surge occurred in the Korean Peninsula. The Ural, Okhotsk, and North Atlantic regions show high blocking frequency when a cold surge occurs over the Korean Peninsula at the same time (solid line in Figure 2a). In particular, the blocking frequency in the Ural and Okhotsk regions is up to 2.7 times higher than the mean blocking frequency in winter (Figure 2b). When blocking and cold surges coincide for more than 1 day, they are defined as blocking type cold surges (B_CS). In this study, to investigate cold surges affected by the blocking location, blocking that occur at 45°E–90°E and 90°E–150°E at latitudes between 40°N and 80°N are referred to as UR blocking (UR_B) and OK blocking (OK_B), respectively. The case when UR_B and OK_B occur simultaneously or continuously is referred to as DO_B. In addition, cold surges that occurred irrespective of blocking are defined as non-blocking type cold surges (nB_CS).

Table 1 lists the characteristics of the four types of cold surges, such as the occurrence frequency and duration, intensity of the cold surge (Ics) which are identified by an analysis of 56 ASOS data in South Korea. The Ics is defined as the mean temperature anomalies throughout the cold surge. B_CS account for approximately 20% of all cases of cold surges, and the durations of the B_CSs are 1–9 days longer than those of nB_CS. The Ics of B_CS are stronger than nB_CS, ranging from 1.3 to 2.5°C. Overall, on average, B_CS is characteristically stronger and lasts longer than nB_CS, even though most cold surges are caused by nB_CS. OK_CS shows the highest number of occurrences of B_CS, followed in order by UR_CS and DO_CS. OK_CS comprise 51% of the total B_CSs, and UR_CS and DO_CS account for 38 and 11%, respectively. DO_CS has the longest duration, followed by OK_CS and UR_CS. With respect to the Ics value, DO_CS shows the highest Ics value, followed in order by UR_CS and OK_CS. Overall, the characteristics of the cold surges are related to the presence of blocking, and the characteristics of B_CS also differ according to the blocking location. Although the numbers of cases classified as UR_CS, OK_CS, and DO_CS are not sufficient to draw statistical conclusions, each B_CS classified in this study shows some common characteristics. For example, in the case of the four DO_CSs, as shown in Z500 (Figure S1), blockings are located simultaneously in Ural

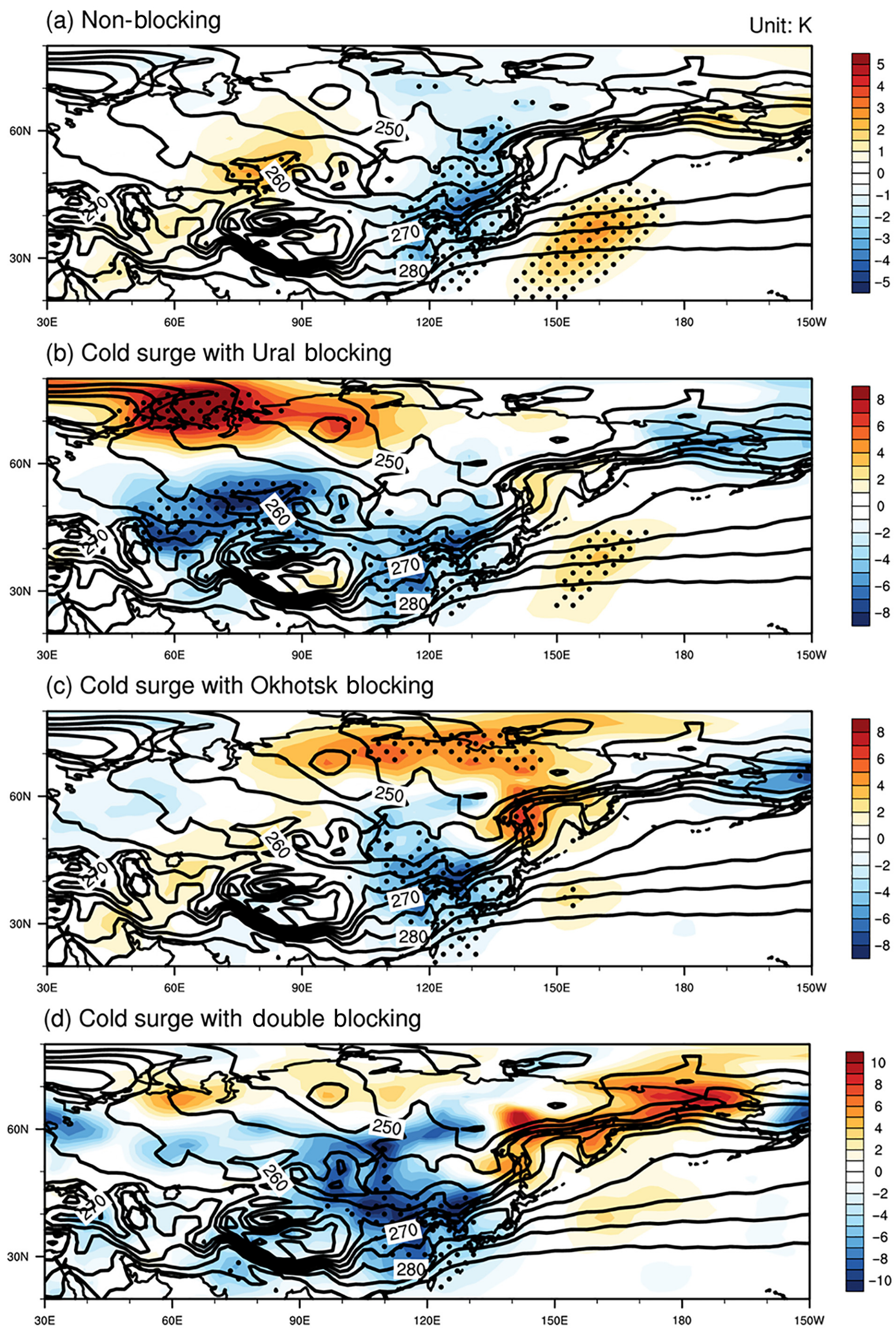


**FIGURE 4** Composite of T2m anomalies (shading; significant values at 99% confidence level indicated by black dots), and climatology of T2m solid lines; contour interval of 5K) for (a) nB_CS, (b) UR_CS, (c) OK_CS, and (d) DO_CS cases [Colour figure can be viewed at wileyonlinelibrary.com]

and Okhotsk between Day −2 and Day 0, after which Okhotsk blocking retrogresses and merges with Ural blocking.

Figure 3 presents a box plot showing the distribution of the Ics, and duration of each type of cold surge. In terms of intensity and duration, the characteristics of the four types of cold surges are more clearly distinguished. Overall, B_CS is stronger and lasts longer than nB_CS. Among the B_CSs, UR_CS and OK_CS have similar median Ics values, but the top 25th percentile of the Ics values of UR_CS is 0.7°C higher than those of OK_CS. There is once a case in which a wave-type cold surge passes through the Korean Peninsula twice in a row. During this period, an unusually long and cold surge (∼13-day-long) continues in the region.

## 3.2 | Composite analysis for each type of CS

The composite map shows the anomalous temperature at 2 m (T2m) for the four types of cold surges classified

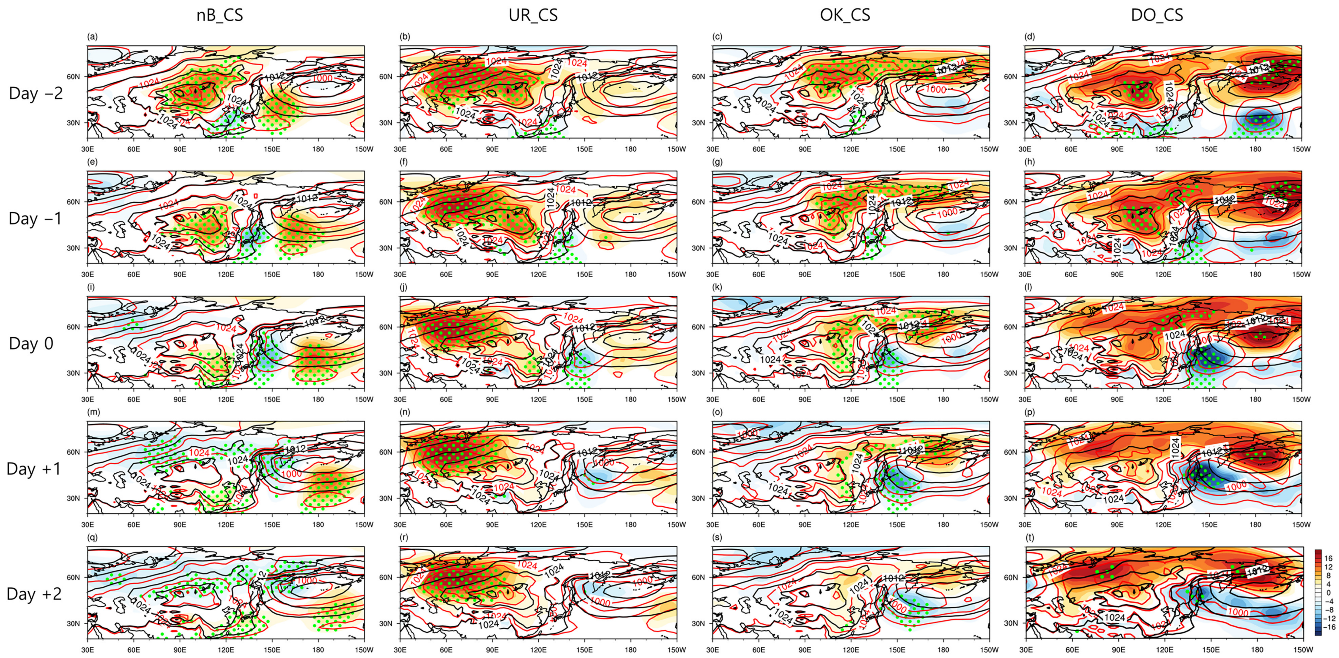


**FIGURE 5** Composite of SLP anomalies (shading; significant values at 99% confidence level indicated by green dots), composite of SLP (indicated by the solid red lines), and climatology of SLP (indicated by solid black lines) for Day −2 to Day +2 related to nB_CS (a, e, i, m, q), UR_CS (b, f, j, n, r), OK_CS (c, g, k, o, s), and DO_CS (d, h, l, p, t). The contour interval is 6 hPa [Colour figure can be viewed at wileyonlinelibrary.com]

in this study (Figure 4). Anomalies have been calculated from the 42 winter averages of each variable. The statistical significance of composite maps is evaluated using the two-tailed Student's *t*-test. For nB_CS, a positive anomaly is observed in the Northwest Pacific and the central regions of the Eurasian continent, and a negative anomaly appears centred at around the Korean Peninsula, showing a distinct wave-train pattern (Figure 4a). In this regard, nB_CS can be considered the wave-train type cold surge as defined by Park *et al.* (2014). For UR_CS, a positive anomaly is observed in the Kara Sea, and a negative anomaly appears in the central regions of the Eurasian continent, showing a meridional dipole pattern in the Ural region with the negative anomaly extending from the Eurasian continent to the Korean Peninsula and Japan (Figure 4b). In OK_CS, a positive anomaly is observed in the Eastern Siberia and Okhotsk regions, and a negative anomaly is located in Northeast Asia, showing a dipole pattern in the meridional direction (Figure 4c). Regarding DO_CS, a strong negative anomaly is observed in most of the East Asia region, and a positive anomaly appears in the Okhotsk region and around the Bering Strait (Figure 4d). Four types of cold surges are considered to have different characteristics because the T2m shows different distribution depending on what type of blocking influences the cold surge.

Figure 5 presents a composite map of the SLP, anomalous SLP, and climatology of SLP to assess the spatial change in the SLP from 2 days before initiation of the cold surge (Day −2) to 2 days after initiation of the cold surge (Day +2). In the case of nB_CS, the Siberian high is strengthened around Mongolia on Day −2. A negative anomaly appears around the Korean Peninsula and in the eastern part of China, with a positive anomaly in the east of Japan, showing a wave-train pattern (Figure 5a). Between Day −1 and the initiation day of the cold surge (Day 0), the Siberian high is weakened gradually and expands towards the Korean Peninsula and the eastern part of China. At the same time, the negative anomaly that spans the Korean peninsula and the positive anomaly in the eastern part of Japan also moves eastward. In this case, the pressure gradient in the Korean Peninsula is strengthened between the positive anomaly over eastern China and the negative anomaly is located to the east (Figure 5e,i). Between Day +1 and Day +2, all anomalies are weakened rapidly: the positive anomaly located to the east of the Korean Peninsula continues to move eastward. The negative anomaly becomes very weak while moving northeast towards the Kamchatka Peninsula (Figure 5m,q).

Regarding UR_CS, a strong positive SLP anomaly appears in a relatively wide area from the Ural region to the region around Lake Baikal on Day −2 (Figure 5b).

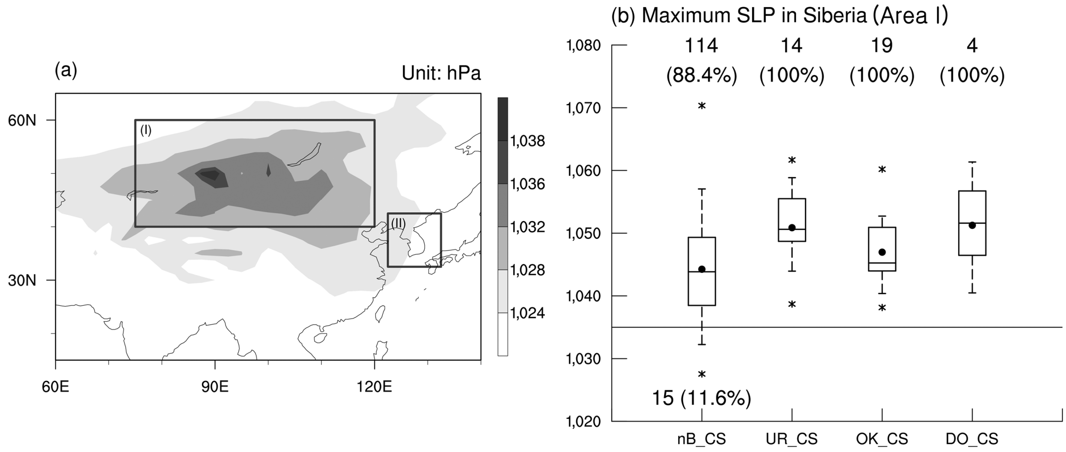


**FIGURE 6** (a) Climatological SLP during DJF (shading), Siberian high domain (Area I), and Korea peninsula domain (Area II). (b) Same as Figure 4, but for the maximum SLP in Area I

These anomalies related to UR_B and the Siberian high expands towards eastern China during Day −1 and Day 0. The anomaly around Lake Baikal is weakened, and a significant anomaly is observed only in the Ural region and the eastern part of China. As in nB_CS, a negative anomaly develops in the eastern part of Japan, and the pressure gradient becomes strong around the Korean Peninsula (Figure 5f,j). During Day +1 and Day +2, the positive anomaly expands to the eastern part of China. The negative anomaly in the eastern part of Japan moves towards the Kamchatka Peninsula in the northeast weakened significantly. On the other hand, the positive SLP anomaly in the Ural region is maintained, and UR_B continues even after Day +2 (Figure 5n,r).

As for OK_CS, a strong positive SLP anomaly appears from Lake Baikal to the Bering Strait on Day −2 (Figure 5c). In the case of nB_CS and UR_CS, the positive anomaly moves southeast and expands towards the eastern part of China. By contrast, in OK_CS, the anomaly moves south and expands to eastern China between Day −1 and Day 0. At the same time, a negative SLP anomaly develops around Japan, making the pressure gradient around the Korean peninsula stronger (Figure 5g,k). During Day +1 and Day +2, the Siberian high, which expands to eastern China, continues to weaken but is still statistically significant. The negative SLP anomaly located mainly around Japan cannot move in a northeast direction as in the cases of nB_CS and UR_CS, and remains strong in place. This is because OK_B remains strong and blocks the movement of the negative SLP anomaly eastward. Consequently, the pressure gradient over the Korean Peninsula also continues to remain strong (Figure 5o,s).

DO_CS shows the combined characteristics of OK_CS and UR_CS. On Day −2, a strong positive SLP anomaly centred around Lake Baikal and the Bering Strait appears (Figure 5d). The Siberian high around Lake Baikal already expands to the eastern part of China on Day −1, and a negative anomaly develops around Japan, strengthening the pressure gradient around the Korean peninsula (Figure 5h). Between Day 0 and Day +2, the positive SLP anomaly distributes throughout Eurasia and across Bering Strait with little change in the pattern. The negative anomaly located mainly around Japan becomes stronger and expands gradually eastward (Figure 5l,p,t). During this period, the positive SLP anomaly in a high-latitude region extends over an elongated area from the Ural region to the Bering Strait. The positive anomaly appears in a relatively wide area from the Ural region to the region around Lake Baikal and from Lake Baikal to the Bering Strait, respectively, as in the case of UR_CS and OK_CS. Accordingly, the anomaly represents a combined pattern of UR_B and OK_B. As the negative SLP anomaly remains strong, the pressure gradient around the Korean peninsula also remains strong.

## 3.3 | Siberian high and CS

When the Siberian high develops and expands, the Korean Peninsula is located on the edge of the Siberian high and the Aleutian low in the east. As a result, the pressure gradient becomes strong in the region, which induces a strong northerly wind, leading to a sharp temperature drop due to strong cold temperature advection (Zhang *et al.*, 1997; Gong and Ho, 2002; Jhun and Lee, 2004; Chang and Lu, 2012).

Regardless of the type of cold surge, it is commonly observed that when a cold surge occurs over the Korean peninsula, the Siberian high expands, the pressure

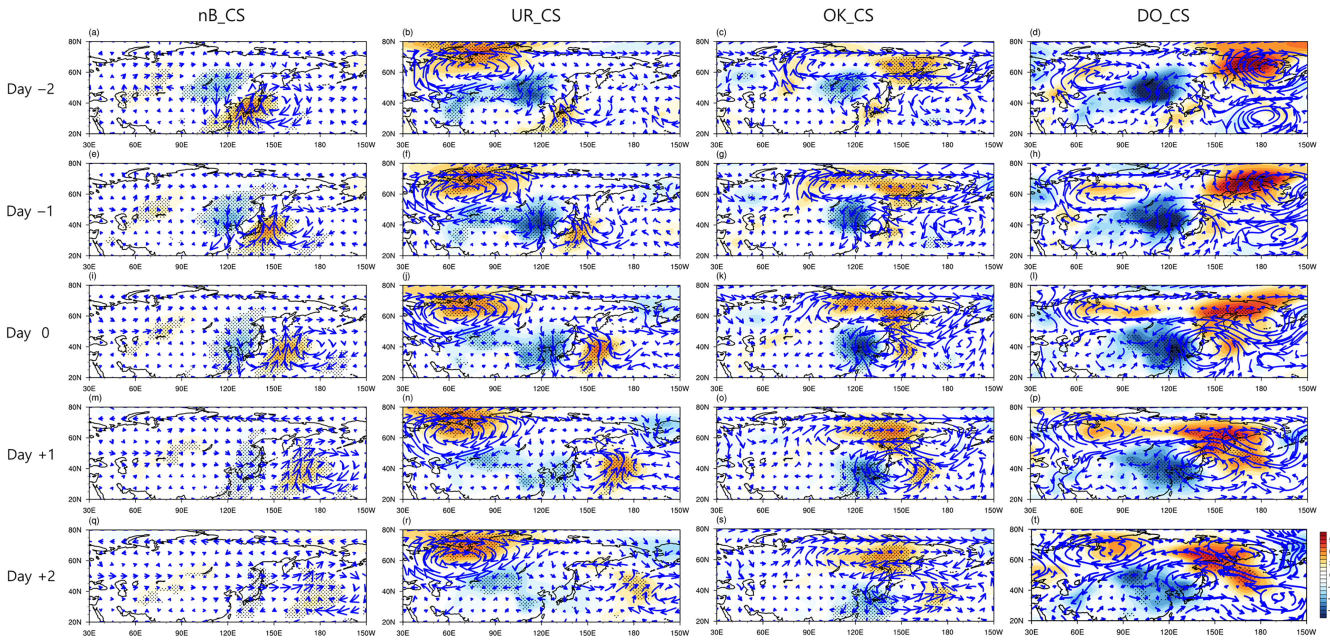


**FIGURE 7** Composite of the T850 anomalies (shading with contour; significant values at 99% confidence level indicated by black dots) and UV850 (vector) for Day −2 to Day +2 related to nB_CS (a, e, i, m, q), UR_CS (b, f, j, n, r), OK_CS (c, g, k, o, s), and DO_CS (d, h, l, p, t) [Colour figure can be viewed at wileyonlinelibrary.com]

gradient around the Korean Peninsula becomes stronger, and a negative SLP anomaly passes through the Korean peninsula. In the case of nB_CS, however, the negative SLP anomaly tends to move relatively fast. On the other hand, when B_CS occurs, the pressure gradient around the Korean Peninsula becomes stronger and remains longer than when nB_CS occurs. In addition, SLP anomalies persist for a relatively long period when B_CS occurs. Another difference among the four B_CS is that the SLP anomaly remains strong until Day +2 in the Ural region in the case of UR_CS, in the Okhotsk region for the OK_CS, and both the Ural and Okhotsk regions for the DO_CS.

All four types of cold surges are related to the Siberian high. Most studies consider the development and expansion of the Siberian high when classifying the East Asian cold surges and claim that when the maximum SLP in the Siberian area (40–60°N, 75–110°E) exceeds 1,035 hPa, it affects the cold surge over the Korean Peninsula (Zhang *et al.*, 1997; Chen *et al.*, 2004; Park *et al.*, 2010a; 2014; 2015). The degree to which the type of cold surges are affected by the Siberian high is examined by setting the Siberian high area to Area I in Figure 6a (40–60°N, 75–110°E) (Gong and Ho, 2002; Wu and Wang, 2002; Jhun and Lee, 2004; Chang and Lu, 2012). Figure 6b shows the maximum SLP in Area I at Day 0. The upper and lower numbers represent the number and ratio of cold surges related and unrelated to the strengthening of the Siberian high, respectively, by a cold surge type. All 37 B_CSs are associated with the strengthening of the Siberian high as the SLP exceeded 1,038 hPa at the time of occurrence. In particular, when UR_CS and DO_CS occur, the average SLPs are relatively high. In the case of nB_CS, it shows the lowest strength on average, but the upper 95th percentile is 1,057 hPa, and the maximum pressure reaches 1,070 hPa. This means that nB_CS can be associated more strongly with the Siberian high than in the case of B_CS. Although 15 out of 129 nB_CSs (11.6%) are not related to the strong Siberian high, cold surges on the Korean Peninsula are generally associated with the strong development of high pressure in Area I.

## 3.4 | Vertical structure and baroclinicity of CS

Figure 7 shows the anomalous wind (W850) and anomalous temperature (T850) in the 850 hPa composite map illustrating the low-level atmospheric pattern for each cold surge. Although each of the four types of cold surges has its distinct characteristics, there are several common patterns are shared by the four types of cold surges. On Day −2, the northerly wind anomaly and negative T850 anomaly are observed around Lake Baikal. To the east of the Korean peninsula, the wind anomaly rotates clockwise. As a result, a southerly wind anomaly appears over the Korean peninsula. From Day −1 to Day 0, all patterns

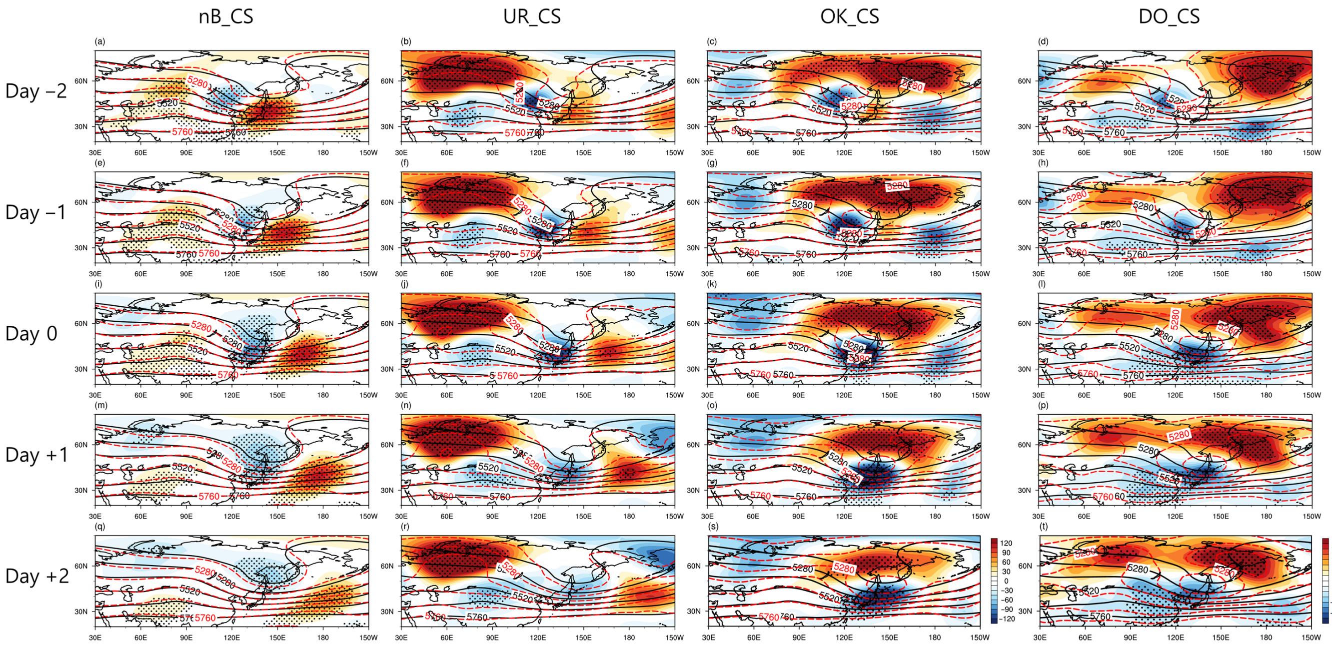


FIGURE 8 Same as Figure 5. But for Z500. Composite of Z500 anomalies (shading; significant values at 99% confidence level indicated by black dots), composite of SLP (indicated by the dotted red lines), and climatology of SLP (indicated by solid black lines). The contour interval is 120 m [Colour figure can be viewed at wileyonlinelibrary.com]

observed in each cold surge move to the southeast. The W850 anomaly rotating clockwise, which is located east of the Korean Peninsula, moves southeastward. Therefore, the regions affected by the southerly wind anomaly and negative T850 move southeastward. In addition, the northerly wind anomaly and negative T850 anomaly present around Lake Baikal move in a southeast direction towards the Korean Peninsula and thus are located around the Korean Peninsula. All types of cold surges commonly show a pattern in which a northerly wind anomaly is located around the Korean peninsula, and cold air moves southward.

The difference among the four types of cold surges is that, in the case of nB_CS, there are positive anomalies in Central Asia and southeast of South Korea, showing a wave-train pattern (Figure 7a). The patterns move eastward more quickly than in the other types of cold surges. On Day +1, the northerly wind anomaly and negative T850 anomaly around the Korean peninsula are already weakened. On Day +2, they leave the Korean Peninsula and almost disappear (Figure 7m,q).

As for the UR_CS, the W850 anomaly rotating clockwise appears around the Ural region. A negative T850 anomaly near Lake Baikal is formed over a wide area of Central Asia due to the northerly wind anomaly. A positive T850 anomaly is formed over a wide area in the Barents-Kara Sea because of the southerly wind anomaly. The northerly wind anomaly and negative T850 anomaly around the Korean Peninsula remain relatively strong until Day +1 compared to nB_CS. On Day +2, the anomalies around the Korean peninsula move to the east and became very weak. However, the W850 anomaly in the Ural region and the T850 anomaly near the Barents-Kara Sea are maintained from Day +1 to Day +2 (Figure 7n,r).

In OK_CS and DO_CS, the W850 anomaly rotating clockwise appears around the Bering Sea, and the positive T850 anomaly appears in the eastern part of Russia. From Day −2 to Day +2, anomalies in the regions where blocking is located continue to be maintained. In the case of DO_CS, the size of the anomaly is relatively larger and stronger. The W850 anomaly located east of the Korean peninsula does not move eastward and remains in place, continuously maintaining a northerly wind anomaly and supplying cold air to the Korean peninsula. Therefore, the negative T850 anomaly also remains strong until Day +2 (Figure 7o,s). In the case of DO_CS, similar to OK_CS, the anomalies around the Korean peninsula are stagnant, and the northerly wind anomaly and negative T850 anomaly continue to be maintained around the Korean peninsula. (Figure 7p,t).

Figure 8 presents a composite map of the geopotential height at 500 hPa (Z500), anomalous Z500, and climatology of Z500 to examine the spatial changes in the middle atmosphere from Day −2 to Day +2. In the case of nB_CS, a negative Z500 anomaly appears in the northeastern part of China on Day −2, strengthening the trough. A positive anomaly appears in Central Asia and Japan building up the ridge, showing a wave-type pattern

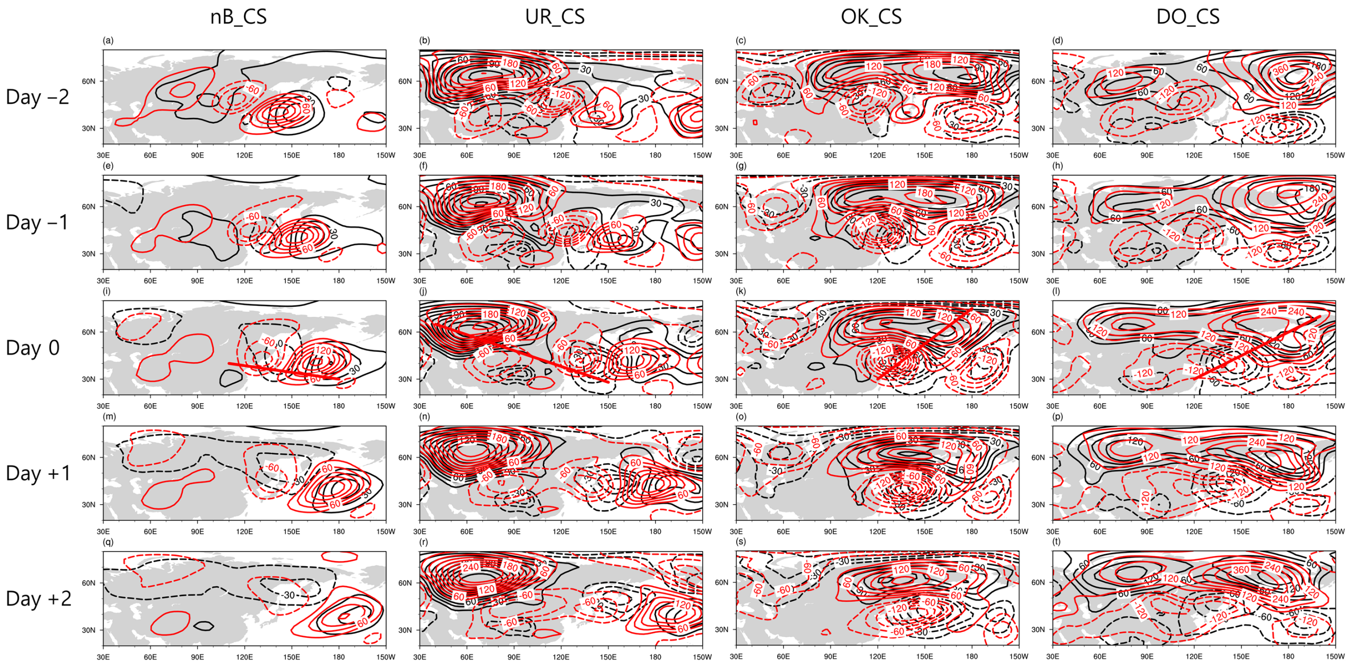


**FIGURE 9** Composite of Z850 anomalies (black lines) and Z300 anomalies (red lines) for Day −2 to Day +2 related to nB_CS (a, e, i, m, q), UR_CS (b, f, j, n, r), OK_CS (c, g, k, o, s), and DO_CS (d, h, l, p, t). Contour interval of 15 m (DO CS has 30 m) at Z850 and 30 m (DO_CS has 60 m) at Z300. The dashed lines indicate negative values [Colour figure can be viewed at wileyonlinelibrary.com]

(Figure 8a). Between Day −1 and Day 0, the negative anomaly and trough reach the Korean Peninsula, and their intensity is increased, reaching a peak (Figure 8e,i). Subsequently, from Day +1 to Day +2, the negative anomaly moves northeast towards the Kamchatka Peninsula, gradually weakening, and the positive anomaly continues to move eastward and be weakened. The positive anomaly in Central Asia is weakened, moving southward (Figure 8m,q).

In the case of UR_CS, from Day −2, the strong positive Z500 anomaly is located around the Ural area. In Inner Mongolia, a negative anomaly and a trough are formed. At this time, a positive Z500 and a weak ridge form around Japan. From Day −1 to Day 0, the negative anomaly and trough in the northeastern part of China move southeast along the isobar. They are located over the Korean Peninsula, and the trough strengthens to the maximum intensity. The positive anomaly around Japan continues to move, and the strong positive anomaly and ridge in the Ural region continue to maintain their positions (Figure 8f,j). While the anomaly in the Ural region maintains its position and intensity in Day +1 and Day +2, the negative anomaly over the Korean Peninsula and the positive anomaly in the east continue to move eastward. However, they move slower than when nB_CS occurs (Figure 8n,r).

Regarding OK_CS, a positive Z500 anomaly appears over a large area of Russia on Day −2: a ridge appears to the west of Lake Baikal, and a negative anomaly and a cut-off low are present in the northeastern part of China (Figure 8c). From Day −1 to Day 0, the positive anomaly at a high latitude is reduced around Okhotsk but its intensity is maintained. During this period, a strong negative anomaly and a strong cut-off low develop around the Korean Peninsula (Figure 8g,k). On Day +1 and Day +2, the positive anomaly shrinks around the Sea of Okhotsk, but its central core remains strong. A negative anomaly or a cut-off low is blocked by the ridge formed in the east and moves very slowly. Even on Day +2, it is still located around Japan and still strong (Figure 8o,s).

In DO_CS, a strong positive anomaly appears near the Bering Strait on Day −2, and a positive anomaly and ridge appear in the Ural region. A deep trough and negative anomaly are located in the northeastern part of China (Figure 8d). From Day −1 to Day 0, the positive anomaly in the Ural region becomes stronger, and the positive anomaly near the Bering Strait expands to the west and south, it is connected to the anomaly in the Ural region. The trough and negative anomaly in the northeastern part of China develop into a cut-off low, becoming stronger, and moving southward to the Korean Peninsula (Figure 8h,l). From Day +1 to Day +2, the positive anomaly in the Ural region becomes stronger and the positive anomaly near the Bering Strait is reduced towards the Okhotsk region. The cut-off low and trough located over the Korean Peninsula are blocked by the anomaly near the Bering Strait and affect the Korean peninsula (Figure 8p,t).

One of the common features in all types of cold surges is that the Korean Peninsula appears to be influenced by the trough. As the trough passes over the Korean Peninsula, cold advection from the north in the middle atmosphere occurs. When each type of cold surge occurs, there is a difference in the intensity of the trough and the speed at which the trough passes through the Korean Peninsula, depending on whether blocking occurs or not and where blocking occurs. In other words, when influenced by B_CS instead of nB_CS, the intensity of the trough is relatively higher, and the movement speed of the trough passing over the Korean Peninsula is lower. In the case of nB_CS, when blocking occurs in the east rather than west of the Korean Peninsula, the movements of the trough are slow due to stagnant atmospheric flow. Accordingly, the blocking type cold surges are ranked in the order of DO_CS, OK_CS, and UR_CS in terms of the intensity of the trough and the speed at which the trough passes over the Korean peninsula.

Figure 9 presents a composite of superimposed Z850 and Z300 anomalies to illustrate the vertical structure of geopotential anomaly distributions. For nB_CS, as the trough related to the cold surge moved southeastward from the Ural region, the wave-train anomalies in the upper and lower atmosphere moves together along the wave-path (Figure 9a,e,i,m,q). The anomalous baroclinicity associated with the trough is at its strongest stage, particularly during Day −1 and Day 0, when the wave trough passes around the Korean Peninsula (Figure 9e,i). Subsequently, the baroclinicity appears to decrease (Figure 9q).

As for UR_CS, the central position of the large positive anomaly in the Ural region remains almost unchanged during the entire period, and its vertical structure is quite barotropic (Figure 9b,f,j,r). However, the wave-train pattern of positive and negative anomalies in the eastern and northwestern parts of the Korean Peninsula, respectively, moves southeastward from Siberia to Korea and Japan, as in nB_CS. Unlike the positive anomaly in the Ural region, where blocking occurs, the pair of anomalies related to the cold surge in the Korean Peninsula has a baroclinic structure. Interestingly, the negative anomaly located to the south of the positive anomaly in the Ural region (Figure 9b), having a baroclinic structure, continues to be connected zonally to the negative anomaly of the pair after the cold surge passed the Korean Peninsula (Figure 9n,r). This connection seems to contribute to slow down the trough passing through the Korean Peninsula, unlike the nB_CS case.

In OK_CS, a positive anomaly appears in the same location vertically in the upper and lower atmospheres over a wide area centred on the eastern part of Russia from Day −2, indicating a barotropic structure. A negative anomaly appears in both the upper and lower atmospheres around the northwest of the Korean peninsula. However, it is tilted in a southeast-northwest direction vertically, indicating a baroclinic structure (Figure 9c). The positive anomaly, which is located over a wide area at a high latitude, continues to maintain its position, but the baroclinic anomaly near the Korean peninsula moves gradually southward and is centred around the Korean peninsula on Day −1 (Figure 9g). From Day 0, however, the positive anomaly in the north expands to the Sea of Okhotsk, blocking the movement of the negative anomaly. The negative anomaly remains around the Korean peninsula for a relatively long time, increasing the vertical tilt (Figure 9k,o,s).

DO_CS shows a pattern that appears to be a combined representation of both UR_CS and OK_CS. On Day −2, vertically straight barotropic anomalies in the upper and lower atmospheres appear in the Ural area and near the Bering Strait. At the same time, negative anomalies appear in a very complex pattern in the mid-latitude (Figure 9d). Throughout the entire period, the positive anomalies in the high latitudes continue to remain in place. On the other hand, negative anomalies appear around the eastern part of the Korean Peninsula in the lower atmosphere and over a wide area from the northwestern part of the Korean Peninsula to most regions of China in the upper atmosphere. Subsequently, these baroclinic negative anomalies around the Korean peninsula move eastward gradually, but they are blocked by the positive anomaly extending from the Bering Strait to the Northwest Pacific and continue to be located around the Korean Peninsula (Figure 9l,p,t).

In nB_CS, the baroclinic structure passes quickly through the Korean peninsula, causing a cold surge. As for B_CS, on the other hands, blocking remains in place and maintains the barotropic structure. The negative anomalous baroclinic structure derived from blocking passes slowly over the Korean peninsula due to blocking.

## 3.5 | AO and CS

As mentioned in the introduction, there are many studies showing that the wintertime cold weather on the Korean Peninsula is largely affected by AO (e.g., Gong *et al.*, 2001; Gong and Ho, 2004; Im and Ahn, 2004; Jeong and Ho, 2005; Hong *et al.*, 2008; Kim and Ahn, 2010; Park *et al.*, 2010b; Woo *et al.*, 2012; Park and Ahn, 2016). Accordingly, the relationship between the four types of cold surges and AO was investigated. The AO index used in this analysis was provided by NOAA CPC at

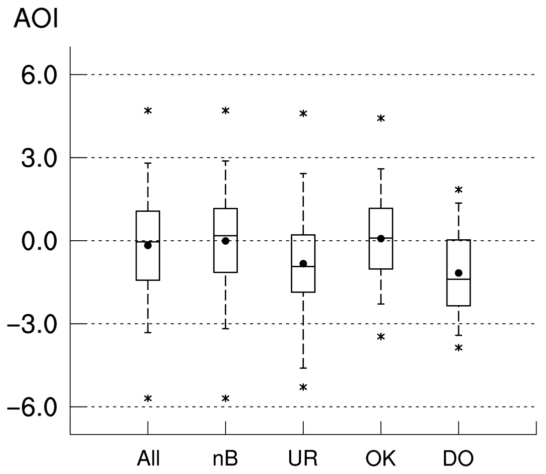


FIGURE 10 Same as Figure 3 but for the Arctic oscillation index. the values are from CPC

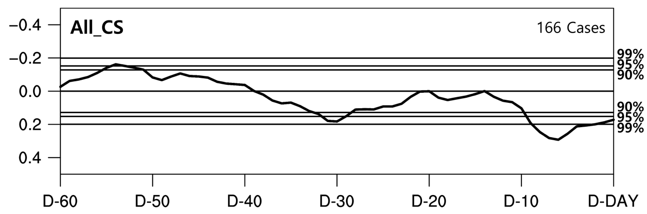


FIGURE 11 Lag-correlation between the surface temperature when a cold surge occurred over South Korea and AOI for Day−60 to Day 0. The percentages on the right side of the graph indicate statistically significant level

https://www.cpc.ncep.noaa.gov/products/precip/CWlink/daily_ao_index/ao.shtml. Figure 10 presents the magnitude of the AO index during the four types of cold surge. When nB_CS, UR_CS, OK_CS, and DO_CS occur, the medians of the AO index are 0.2, −0.9, 0.1, and − 1.4, respectively. While the medians of UR_CS and DO_CS have negative AO indices, nB_CS and OK_CS appear to occur regardless of the AO phase. According to the daily lag-correlation between the AO index and the surface temperature of the Korean Peninsula, however, the cold surge in the region has a 50–60-day lag-correlation with the AO index, which is significant at the 95% confidence level in two-tailed tests (Figure 11). Indeed, many studies have shown (e.g., Im and Ahn, 2004; Jeong and Ho, 2005; Kim and Ahn, 2010; Park and Ahn, 2016) that the average winter temperature on the Korean Peninsula is largely warm and cold during the positive and negative AO phases, respectively. That is, although the occurrence of a cold surge in the region does not appear to have a significant simultaneous daily relationship with the AO, there is a clear lag-correlation between the occurrence of cold surge and AO. These results differ from Jeong and Ho (2005) and Park *et al.* (2014), who have not classified and examined cold surge, as in this study. The relationship between the AO and boreal wintertime blocking for cold surge is beyond the scope of this study, and further research will be needed.

## 4 | SUMMARY AND CONCLUSION

This study examine the characteristics of cold surges in the Korean Peninsula over the last 45 years (1975–2019). Of the 166 cases of cold surges that occurred during the period, 78% of the cold surges are associated with the passage of a wave-train type baroclinic trough moving southeastward from the northwest across the Korean Peninsula (nB_CS), and the rest of surges are influenced by blocking (B_CS). Although blocking has not been identified clearly, studies have shown that it has many causes (Shutts, 1983; Mullen, 1987; Nakamura and Wallace, 1993; Li, 2004; Nakamura and Fukamachi, 2004; Sato *et al.*, 2014; Lim, 2015; Luo *et al.*, 2016; Jin *et al.*, 2020; Tyrlis *et al.*, 2020), and blocking can cause abnormally low temperatures in an area (Park *et al.*, 2014, 2015; Bae and Min, 2016; Choi and Kim, 2016). The blockings causing cold surges over the Korean peninsula occur mostly around the Sea of Okhotsk and Ural region (OK_B and UR_B, respectively). In rare cases, blocking occurs simultaneously in the two regions (DO_B), causing strong and long-lasting cold surges. Because the cold surges on the Korean Peninsula are affected by the location as well as the occurrence of blocking, this study divided B_CS into three types (UR_CS, OK_CS, and DO_CS) and examined the characteristics of each type, including nB_CS. Although the numbers of cases classified as UR_CS, OK_CS, and DO_CS are not sufficient to draw statistical conclusions, each B_CS classified in this study exhibits common characteristics.

Although most of the cold surges occurring in the region are nB_CSs, and the cases of B_CS are relatively small, B_CS show a stronger intensity that lasts longer than nB_CS. The mean duration of nB_CS, UR_CS, OK_CS, and DO_CS are 2.7, 3.6, 5.1, and 11.8 days, respectively, and the mean intensity values of nB_CS, UR_CS, OK_CS, and DO_CS are −3.8, −5.4, −5.1, and − 6.3°C, respectively. Therefore, despite the small number of occurrences of B_CS, they tend to bring about relatively strong cold surges. Because blocking has a barotropic structure and, when it occurs, lasts for 1 week or longer (Rex, 1950), the blocking that influenced the cold surge over the Korean Peninsula tends to last for a relatively long period compared to nB_CS because the trough is continually linked to the blocking behind, as in the case of UR_CS, or the movement of the trough is stagnated by the blocking ahead, as in the case of OK_CS. In particular, in the case of OK_CS, blocking is located to the east of the cold surge, and the movement of the cold surge is the slowest. On the other hand, in nB_CS, the cold surge duration is the shortest because the trough related to the wave-train moves rapidly. In short, the intensity and movement speed of the trough related to the cold surge vary according to the presence and location of blocking.

All four types of cold surges that occurred in the Korean Peninsula are related to the passage of a trough with a baroclinic structure and a cold front that resulted in cold advection from northwest to the southeast. Although blocking that affected the cold surge in the Korean Peninsula has a barotropic structure, the trough caused by the blocking is baroclinic.

All four types of cold surges classified in this study are related to the expansion of the Siberian high. Regardless of the type of cold surge, when a cold surge occurs over the Korean peninsula, the Siberian high expands, the pressure gradient around the Korean Peninsula becomes stronger, and a negative SLP anomaly passes through the Korean peninsula. In the case of nB_CS, however, the negative SLP anomaly tends to move relatively quickly. On the other hand, when B_CS occurs, the pressure gradient around the Korean Peninsula becomes stronger and remains longer than when nB_CS occurs owing to the influence of blocking. In addition, UR_CS and DO_CS are more closely related to the Siberian high expansion than OK_CS and nB_CS.

The relationship between the four types of cold surges and AO was investigated. According to the daily lag-correlation between the AO index and the surface temperature of the Korean Peninsula, the cold surge in the region has a 50–60-day lag-correlation with the AO index, which is significant at the 95% confidence level. The analysis has something in common in that the average winter temperature of the Korean Peninsula has a significant correlation with the AO, as many studies have shown (e.g., Im and Ahn, 2004; Jeong and Ho, 2005; Kim and Ahn, 2010; Park and Ahn, 2016), although there is no clear simultaneous correlation between the occurrence of CS and the AO based on the daily data.

All types of cold surges appear to be influenced by the trough. When each type of cold surge occurs, however, there is a difference in the intensity of the trough and the speed at which the trough passes through the Korean Peninsula depending on whether blocking occurs and where the blocking occurs. In other words, when influenced by B_CS instead of nB_CS, the intensity of the trough is relatively higher, and the movement speed of the trough passing through the Korean Peninsula is slower. In the case of B_CS, the movements of the trough are slower when blocking occurs in the east of the Korean Peninsula than the west due to stagnant atmospheric flow. Accordingly, the blocking type cold surges are ranked in the order of DO_CS, OK_CS, and UR_CS in terms of the intensity of the trough and the speed at which the trough passes through the Korean peninsula. However, in the case of DO_CS, because there are only four cases, it is necessary to examine its characteristics through a case study in the future.

## ACKNOWLEDGEMENTS

This work was funded by the Korea Meteorological Administration Research and Development Program under Grant KMI2020-01411.

## ORCID

*Eung-Sup Kim* https://orcid.org/0000-0002-3632-5849
*Joong-Bae Ahn* https://orcid.org/0000-0001-6958-2801

## REFERENCES

Bae, J.H. and Min, K.H. (2016) Analysis of the February 2014 East Coast heavy snowfall case due to blocking. *Atmosphere*, 26(2), 227–241 . (in Korean with English abstract). https://doi.org/10.14191/Atmos.2016.26.2.227.

Barnett, A.G., Hajat, S., Gasparrini, A. and Rocklöv, J. (2012) Cold and heat waves in the United States. *Environmental Research*, 112, 218–224. https://doi.org/10.1016/j.envres.2011.12.010.

Barriopedro, D., García-Herrera, R., Lupo, A.R. and Hernández, E. (2006) A climatology of Northern Hemisphere blocking. *Journal of Climate*, 19(6), 1042–1063. https://doi.org/10.1175/JCLI3678.1.

Branstator, G. (2002) Circumglobal teleconnections, the jet stream waveguide, and the North Atlantic oscillation. *Journal of Climate*, 15(14), 1893–1910. https://doi.org/10.1175/1520-0442(2002)015<1893:CTTJSW>2.0.CO;2.

Chang, C.P. and Lu, M.M. (2012) Intraseasonal predictability of Siberian high and east Asian winter monsoon and its interdecadal variability. *Journal of Climate*, 25(5), 1773–1778. https://doi.org/10.1175/JCLI-D-11-00500.1.

Chen, T.C., Yen, M.C., Huang, W.R. and Gallus, W.A. (2002) An east Asian cold surge: case study. *Monthly Weather Review*, 130(9), 2271–2290. https://doi.org/10.1175/1520-0493(2002)130<2271:AEACSC>2.0.CO;2.

Chen, T.C., Huang, W.R. and Yoon, J.H. (2004) Interannual variation of the east Asian cold surge activity. *Journal of Climate*, 17(2), 401–413. https://doi.org/10.1175/1520-0442(2004)017<0401:IVOTEA>2.0.CO;2.

Cheung, H.H.N. and Zhou, W. (2016) Simple metrics for representing east Asian winter monsoon variability: Urals blocking and western Pacific teleconnection patterns. *Advances in Atmospheric Sciences*, 33, 695–705. https://doi.org/10.1007/s00376-015-5204-6.

Choi, W. and Kim, Y.A. (2016) Relationship between the east-Asian cold anomalies in winter of 2010/11 and blocking. *Atmosphere*, 26(1), 193–201. (in Korean with English abstract). https://doi.org/10.14191/Atmos.2016.26.1.193.

Gong, D.Y. and Ho, C.H. (2002) The Siberian high and climate change over middle to high latitude Asia. *Theoretical and Applied Climatology*, 72, 1–9. https://doi.org/10.1007/s007040200008.

Gong, D.-Y., & Ho, C.-H. (2004). Intra-seasonal variability of wintertime temperature over East Asia. *International Journal of Climatology*, 24(2), 131–144. https://doi.org/10.1002/joc.1006

Gong, D.-Y., Wang, S.-W. and Zhu, J.-H. (2001) East Asian winter monsoon and Arctic oscillation. *Geophysical Research Letters*, 28(10), 2073–2076. https://doi.org/10.1029/2000GL012311.

Heo, J.-W., Ho, C.-H., Park, T.-W., Choi, W., Jeong, J.-H. and Kim, J. (2018) Changes in cold surge occurrence over East Asia in the future: role of thermal structure. *Atmosphere*, 9(6), 222. https://doi.org/10.3390/atmos9060222.

Hong, C.C., Hsu, H.H., Chia, H.H. and Wu, C.Y. (2008) Decadal relationship between the North Atlantic oscillation and cold surge frequency in Taiwan. *Geophysical Research Letters*, 35(24), L24707. https://doi.org/10.1029/2008GL034766.

Hu, K., Huang, G., Wu, R. and Wang, L. (2018) Structure and dynamics of a wave train along the wintertime Asian jet and its impact on east Asian climate. *Climate Dynamics*, 51, 4123–4137. https://doi.org/10.1007/s00382-017-3674-1.

Hwang, J., Martineau, P., Son, S., Miyasaka, T. and Nakamura, H. (2020) The role of transient eddies in North Pacific blocking formation and its seasonality. *Journal of the Atmospheric Sciences*, 77(7), 2453–2470. https://doi.org/10.1175/JAS-D-20-0011.1.

Im, E.S. and Ahn, J.B. (2004) Analysis of relationship between Korean winter temperature variability and global circulation indices. *Asia-Pacific Journal of Atmospheric Sciences*, 40(4), 441–452. (in Korean with English abstract).

Jeong, J.H. and Ho, C.H. (2005) Changes in occurrence of cold surges over East Asia in association with Arctic oscillation. *Geophysical Research Letters*, 32(14), L14704. https://doi.org/10.1029/2005GL023024.

Jeong, J.H., Park, T.W., Choi, J.H., Son, S.W., Song, K., Kug, J.S., Kim, B.M., Kim, H.K. and Yim, S.Y. (2016) Assessment of climate variability over East Asia-Korea for 2015/16 winter. *Atmosphere*, 26(2), 337–345. (in Korean with English abstract). https://doi.org/10.14191/Atmos.2016.26.2.337.

Jhun, J.G. and Lee, E.J. (2004) A new east Asian winter monsoon index and associated characteristics of the winter monsoon. *Journal of Climate*, 17(4), 711–726. https://doi.org/10.1175/1520-0442(2004)017<0711:ANEAWM>2.0.CO;2.

Jin, C., Wang, B., Yang, Y.-M. and Liu, J. (2020) "Warm Arctic-cold Siberia" as an internal mode instigated by North Atlantic warming. *Geophysical Research Letters*, 47(9), e2019GL086248. https://doi.org/10.1029/2019gl086248.

Kalnay, E., Kanamitsu, M., Kistler, R., Collins, W., Deaven, D., Gandin, L., Iredell, M., Saha, S., White, G., Woollen, J., Zhu, Y., Chelliah, M., Ebisuzaki, W., Higgins, W., Janowiak, J., Mo, K. C., Ropelewski, C., Wang, J., Leetmaa, A., Reynolds, R., Jenne, R. and Joseph, D. (1996) The NCEP/NCAR 40-year reanalysis project. *Bulletin of the American Meteorological Society*, 77(3), 437–472. https://doi.org/10.1175/1520-0477(1996)077<0437:TNYRP>2.0.CO;2.

Kim, H.J. and Ahn, J.B. (2010) The large-scale atmospheric circulation related to Korea winter temperature variability. *Journal of Climate Research*, 5(2), 118–130. (in Korean with English abstract).

Kim, B.M., Jeong, J.H. and Kim, S.J. (2009) Investigation of stratospheric precursor for the east Asian cold surge using the potential vorticity inversion technique. *Asia-Pacific Journal of Atmospheric Sciences*, 45(4), 513–522.

Kim, B.M., Son, S.W., Min, S.K., Jeong, J.H., Kim, S.J., Zhang, X., Shim, T. and Yoon, J.H. (2014) Weakening of the stratospheric polar vortex by Arctic Sea-ice loss. *Nature Communications*, 5, 4646. https://doi.org/10.1038/ncomms5646.

Lee, D.Y. and Ahn, J.B. (2017) Future change in the frequency and intensity of wintertime North Pacific blocking in CMIP5 modes. *International Journal of Climatology*, 37(5), 2765–2781. https://doi.org/10.1002/joc.4878.

Lejenäs, H. and Økland, H. (1983) Characteristics of northern hemisphere blocking as determined from a long time series of observational data. *Tellus A: Dynamic Meteorology and Oceanography*, 35(5), 350–362. https://doi.org/10.3402/tellusa.v35i5.11446.

Li, S. (2004) Impact of Northwest Atlantic SST anomalies on the circulation over the Ural mountains during early winter. *Journal of the Meteorological Society of Japan*, 82(4), 971–988. https://doi.org/10.2151/jmsj.2004.971.

Lim, Y.-K. (2015) The East Atlantic/West Russia (EA/WR) teleconnection in the North Atlantic: climate impact and relation to Rossby wave propagation. *Climate Dynamics*, 44, 3211–3222. https://doi.org/10.1007/s00382-014-2381-4.

Luo, D., Xiao, Y., Yao, Y., Dai, A., Simmonds, I. and Franzke, C.L. (2016) Impact of Ural blocking on winter warm Arctic–cold Eurasian anomalies. Part I: blocking-induced amplification. *Journal of Climate*, 29(11), 3925–3947. https://doi.org/10.1175/JCLI-D-15-0611.1.

Mullen, S.L. (1987) Transient Eddy forcing of blocking flows. *Journal of the Atmospheric Sciences*, 44(1), 3–22. https://doi.org/10.1175/1520-0469(1987)0442.0.Co;2.

Nakamura, H. and Fukamachi, T. (2004) Evolution and dynamics of summertime blocking over the Far East and the associated surface Okhotsk high. *Quarterly Journal of the Royal Meteorological Society*, 130(599), 1213–1233. https://doi.org/10.1256/qj.03.101.

Nakamura, H. and Wallace, J.M. (1993) Synoptic behavior of baroclinic eddies during the blocking onset. *Monthly Weather Review*, 121(7), 1892–1903. https://doi.org/10.1175/1520-0493(1993)1212.0.Co;2.

Pang, B., Lu, R. and Ren, R. (2020) Influence of Siberian blocking on long-lived cold surges over the South China Sea. *Journal of Climate*, 33(16), 6945–6956. https://doi.org/10.1175/JCLI-D-19-0944.1.

Pang, B., Lu, R. and Ren, R. (2022) Impact of the Scandinavian pattern on long-lived cold surges over the South China Sea. *Journal of Climate*, 35(6), 1773–1785. https://doi.org/10.1175/JCLI-D-21-0607.1.

Park, H.J. and Ahn, J.B. (2016) Combined effect of the Arctic oscillation and the Western Pacific pattern on East Asia winter temperature. *Climate Dynamics*, 46, 3205–3221. https://doi.org/10.1007/s00382-015-2763-2.

Park, T.W., Ho, C.H. and Yang, S. (2010a) Relationship between the Arctic oscillation and cold surges over East Asia. *Journal of Climate*, 24(1), 68–83. https://doi.org/10.1175/2010JCLI3529.1.

Park, T.W., Ho, C.H., Yang, S. and Jeong, J.H. (2010b) Influences of Arctic oscillation and Madden-Julian oscillation on cold surge and heavy snowfalls over Korea: a case study for the winter of 2009–2010. *Journal of Geophysics Research-Atmospheres*, 115, D23122. https://doi.org/10.1029/2010JD014794.

Park, T.W., Ho, C.H. and Deng, Y. (2014) A synoptic and dynamical characterization of wave-train and blocking cold surge over East Asia. *Climate Dynamics*, 43, 753–770. https://doi.org/10.1007/s00382-013-1817-6.

Park, T.W., Ho, C.H., Jeong, J.H., Heo, J.W. and Deng, Y. (2015) A new dynamical index for classification of cold surge types over East Asia. *Climate Dynamics*, 45, 2469–2484. https://doi.org/10.1007/s00382-015-2483-7.

Rex, D.F. (1950) Blocking action in the middle troposphere and its effect upon regional climate. *Tellus*, 2(4), 275–301. https://doi.org/10.3402/tellusa.v2i4.8603.

Ryoo, S.B., Kwon, W.T. and Jhun, J.G. (2004) Characteristics of wintertime daily and extreme minimum temperature over South Korea. *International Journal of Climatology*, 24(2), 145–160. https://doi.org/10.1002/joc.990.

Sato, K., Inoue, J. and Watanabe, M. (2014) Influence of the Gulf stream on the Barents Sea ice retreat and Eurasian coldness during early winter. *Environmental Research Letters*, 9(8), 084990. https://doi.org/10.1088/1748-9326/9/8/084009.

Shutts, G.J. (1983) The propagation of eddies in diffluent jetstreams: Eddy vorticity forcing of 'blocking' flow fields. *Quarterly Journal of the Royal Meteorological Society*, 109(462), 737–761. https://doi.org/10.1002/qj.49710946204.

Tibaldi, S. and Molteni, F. (1990) On the operational predictability of blocking. *Tellus A: Dynamic Meteorology and Oceanography*, 42(3), 343–365. https://doi.org/10.3402/tellusa.v42i3.11882.

Tyrlis, E., Bader, J., Manzini, E., Ukita, J., Nakamura, H. and Matei, D. (2020) On the role of Ural blocking in driving the warm Arctic–cold Siberia pattern. *Quarterly Journal of the Royal Meteorological Society*, 146(730), 2138–2153. https://doi.org/10.1002/qj.3784.

Vavrus, S., Walsh, J.E., Chapman, W.L. and Portis, D. (2006) The behavior of extreme cold air outbreaks under greenhouse warming. *International Journal of Climatology*, 26(9), 1133–1147. https://doi.org/10.1002/joc.1301.

Wang, L., Chen, W., Zhou, W., Chan, J.C.L., Barriopedro, D. and Huang, R. (2010) Effect of the climate shift around mid 1970s on the relationship between wintertime Ural blocking circulation and east Asian climate. *International Journal of Climatology*, 30(1), 153–158. https://doi.org/10.1002/joc.1876.

Woo, S.H., Kim, B.M., Jeong, J.H., Kim, S.J. and Lim, G.H. (2012) Decadal changes in surface air temperature variability and cold surge characteristics over Northeast Asia and their relation with the Arctic oscillation for the past three decades (1979–2011). *Journal of Geophysical Research-Atmospheres*, 117, D18117. https://doi.org/10.1029/2011JD016929.

Wu, B. and Wang, J. (2002) Winter Arctic oscillation, Siberian high and east Asian winter monsoon. *Geophysical Research Letters*, 29(19), 1897–3-4. https://doi.org/10.1029/2002GL015373.

Yang, X., Zeng, G., Zhang, G. and Li, Z. (2020) Interdecadal variation of winter cold surge path in East Asia and its relationship with Arctic Sea ice. *Journal of Climate*, 33(11), 4907–4925. https://doi.org/10.1175/JCLI-D-19-0751.1.

Yang, X., Zeng, G., Zhang, G. and Li, C. (2021) Linkage between interannual variation of winter cold surge over East Asia and autumn sea ice over the Barents Sea. *Theoretical and Applied Climatology*, 144, 339–351. https://doi.org/10.1007/s00704-021-03545-9.

You, J.E. and Ahn, J.B. (2012) The anomalous structures of atmospheric and oceanic variables associated with the frequency of North Pacific winter blocking. *Journal of Geophysical Research-Atmospheres*, 117, D11108. https://doi.org/10.1029/2012JD017431.

Zhang, Y., Sperber, K.R. and Boyle, J.S. (1997) Climatology and interannual variation of the east Asian winter monsoon: results from the 1979–95 NCEP/NCAR reanalysis. *Monthly Weather Review*, 125(10), 2605–2619. https://doi.org/10.1175/1520-0493(1997)125<2605:CAIVOT>2.0.CO;2.

## SUPPORTING INFORMATION

Additional supporting information can be found online in the Supporting Information section at the end of this article.

**How to cite this article:** Kim, E.-S., & Ahn, J.-B. (2023). Study on the classification and characteristics of cold surge in South Korea. *International Journal of Climatology*, *43*(2), 720–735. https://doi.org/10.1002/joc.7820